# Supplementary material

**S1: Details of data used in the study**

| Region | Latitude Bounds | Longitude Bounds | Site names (earliest year of data used, latest year of data used) | No. unique gridcells |
|---|---|---|---|---|
| Brazil (São Paulo) | -26 < Lat < -23 | -58 < Lon< -45 | 'Cubatão-centro (1998, 2015)',<br>'Diadema (1999, 2015)',<br>'Ibirapuera (1998, 2015)',<br>'Ipen (2007, 2015)',<br>'Itaquera (2007, 2015)',<br>'Mauá (1998, 2014)',<br>'Mooca (1998, 2015)',<br>'Nossa Senhora do Ó (2004, 2015)',<br>'Osasco (1998, 2002)',<br>'Parelheiros (2007, 2014)',<br>'Parque D.Pedro II (1998, 2015)',<br>'Pinheiros (1999, 2015)',<br>'S.André-Capuava (2000, 2014)',<br>'San Lorenzo (1996, 2007)',<br>'Santana (1999, 2015)',<br>'Santo Amaro (2002, 2015)',<br>'Sorocaba (2000, 2015)',<br>'São Caetano (1998, 2015)',<br>'São José dos Campos (2000, 2015)',<br>'São Miguel Paulista (1998, 2004)' | 5 |
| Amazonia | -9 < Lat < -2 | -26 < Lon< -23 | 'Amazon KM67 tower (2014, 2015)',<br>'Amazon TT34 tower (2009, 2014)',<br>'GoAmazon T2 (2014, 2015)',<br>'GoAmazon T3 - Manacapuru (2014, 2014)',<br>'Porto Velho (2009, 2012)' | 5 |
| Colombia | 4 < Lat < 7 | -76 < Lon < -74 | 'Buenaventura (2012, 2017)',<br>'C. Alto Rendimiento (2008, 2021)',<br>'Carvajal - Sevillana (2008, 2021)',<br>'Fontibon (2008, 2021)',<br>'Gobernación de Caldas (2014, 2021)',<br>'Guaymaral (2008, 2021)',<br>'Kennedy (2008, 2021)',<br>'Las Ferias (2008, 2021)',<br>'MinAmbiente (2008, 2021)', | 3 |

| | | | | |
|---|---|---|---|---|
| | | | 'Móvil_7ma (2012, 2017)',<br>'Parque Las Aguas (2012, 2017)',<br>'Puente Aranda (2008, 2021)',<br>'San_ Cristobal (2011, 2021)',<br>'Suba (2008, 2021)',<br>'Tunal (2008, 2021)',<br>'Usaquen (2008, 2021)' | |
| South Africa | -27 < Lat < -25 | 27 < Lon < 30 | 'Diepkloof (2007, 2010)',<br>'Ekandustria (2012, 2014)',<br>'Ermelo (2007, 2015)',<br>'Grootvlei (2010, 2015)',<br>'Hendrina (2008, 2015)',<br>'Kliprivier (2007, 2015)',<br>'Mamelodi (2009, 2014)',<br>'Maropeng (2011, 2015)',<br>'Newtown (2004, 2012)',<br>'Olivienhoutbosch (2009, 2014)',<br>'Pretoria west (2009, 2014)',<br>'Randfontein (2012, 2015)',<br>'Randwater (2012, 2015)',<br>'Rosslyn (2009, 2014)',<br>'Sebokeng (2007, 2015)',<br>'Sharpeville (2007, 2015)',<br>'Three Rivers (2007, 2015)' | 6 |
| Ocean (island name) | -20 < Lat < -22 | 55 < Lon < 56 | 'Ecole JOINVILLE (2005, 2013)',<br>'Ecole La Marine (2011, 2013)',<br>'LYC. LISLET GEOFFROY (2000, 2011)',<br>'MONTGAILLARD (2015, 2017)',<br>'STE THERESE (2008, 2010)',<br>'Station Bourg-Murat (2015, 2017)' | 2 |
| DR Congo | 0 < Lat < 4 | 22 < Lon< 12 | 'CONGOFLUX (2020, 2021)',<br>'Bomassa (2001, 2013)',<br>'Zoétélé (2001, 2013)', | 3 |
| West Africa | 6 < Lat < 14 | -6 < Lon < 8 | 'Djougou (2005, 2013)',<br>'Lamto (2001, 2013)', | 2 |

**Table S1: Regions defined for the model evaluation, including all contributing in situ ozone measurement sites. The name or location of the measurement site is listed in the fourth column as well as the earliest and latest year of measurement. The measurements are not necessarily continuous between these periods.**

| **Model variables** | **Variable name** | **Purpose in the study** |
|---|---|---|

| | | |
|---|---|---|
| Ozone mixing ratio | o3 | Used throughout |
| NOx emission rate (including lightning emissions) | eminox, emilnox | Defining 'High-NOx' areas (Section 3.1) |
| OH mixing ratio | oh | Evaluation of future atmosphere ( Section 3.2) |
| Surface temperature | tas | Evaluation of future atmosphere (Section 3.2) |
| Rate of ozone production | o3prod | Ozone budget (Section 3.4) |
| Rate of ozone destruction | o3loss | Ozone budget (Section 3.4) |
| Dry deposition rate | dryo3 | Ozone budget (Section 3.4) |
| NOx ($NO + NO_2$) mixing ratio | no, no2 | Sensitivity test (Section 3.4) |
| Isoprene emission rate | emiisop | Sensitivity test (Section 3.4) |

**Table S2: Variable names and purpose of model data used in the study**

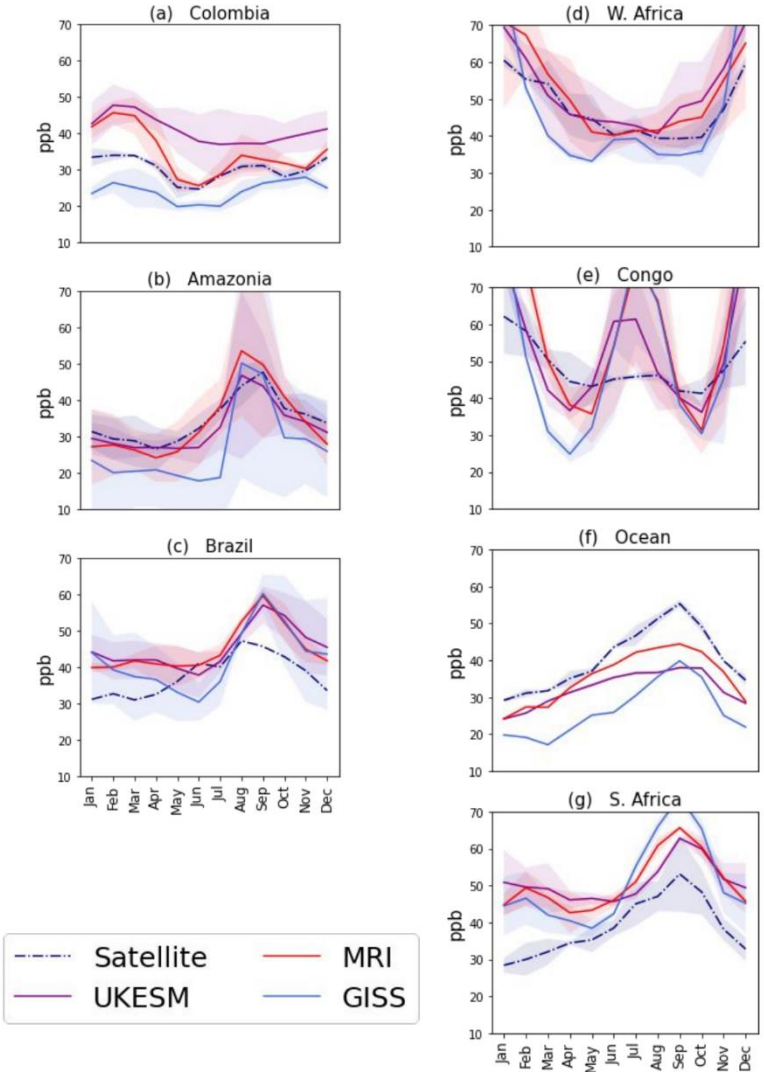


**Figure S1: Monthly mean O3 at the sites defined in Fig. 1. Model means are shown for UKESM1 (purple solid line), GISS (blue solid line) and MRI (red solid line) and 2 standard deviations from the mean are shaded. Model predictions for the period 2015–2020 are taken at 825 hPa (GISS and MRI) and 1.5 km altitude are compared to satellite products from the TES satellite at 825 hPa (navy dash-dot line).**

## S2: Isoprene representation in this paper

In this paper we analyse the relationship between rate of ozone production and isoprene emission rate rather than isoprene concentration. In order to form ozone, emitted isoprene must be oxidised (for example by OH). Once oxidised, the compound is no longer present in the atmosphere as isoprene. This is shown clearly for UKESM1 in Fig. S1 (column 1). Isoprene emissions increase over several areas, however as OH has also increased, this isoprene is effectively oxidised. The result is

that areas with increased isoprene emissions show very little increase in OH or isoprene concentration, but areas where isoprene emissions decrease (e.g. North Amazon) show clear decreases in isoprene concentration, and OH concentrations are higher in this area. Overall, climate change actually causes a decrease in isoprene concentration in UKESM1, even though isoprene emission rate increases. Therefore, isoprene emission rate is likely to better represent the change in isoprene oxidation products.

Figure S1 further exemplifies some of the challenges of climate modelling, and evaluating climate model output. Figure S1 (column 2) shows that although isoprene emissions increase using GISS, this isoprene is not oxidised as efficiently as in UKESM1 because isoprene concentrations also increase. One of the reasons for this is the oxidising capacity of the atmosphere is lower in the GISS model compared to other models. Indeed, Fig. S1 shows that OH concentrations decrease due to climate change over large areas of the land. Model differences such as these are not evaluated in detail in this study although they contribute to differences in concentrations of ozone and precursors between models.

Nonetheless, the trends observed in Figs 6 are not significantly affected by the choice of isoprene emissions or isoprene concentration.

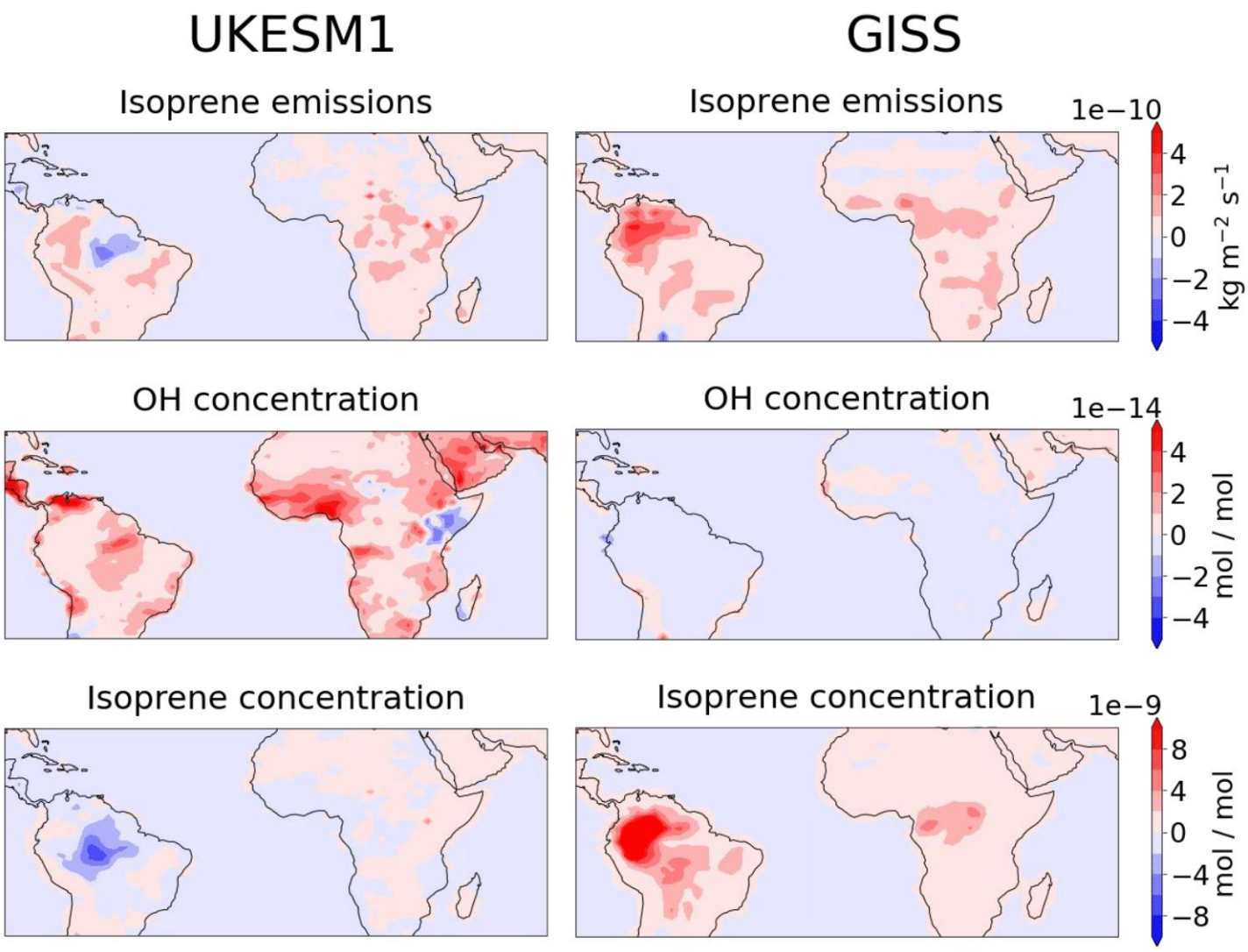


**Figure S2: The average change due to climate change in (top row) isoprene emission rate, (middle row) isoprene concentration and (bottom row) OH concentration for the period 2090 - 2100 for (column 1) UKESM1, (column 2) GISS. Changes are represented for the land surface only.**

## S3: Regional and seasonal surface temperature changes

The largest climate-driven temperature changes occur in the dry seasons (Fig. S2), which coincide with the biomass burning seasons discussed in Sect. 3.3. Surface temperatures increase by 5–5.5 K due to climate change in the Northern Amazon and West Africa in Dec–Feb (Fig. S2a), the central Amazon in June–July (Fig. 2b) and the Southern Amazon and South Africa in Aug–Oct (Fig. 2c). In other seasons, the multimodel mean temperature change is 3.5–4.5 K. Seasonal variation in the Congo is smaller but the maximum temperature increase occurs during June and July.

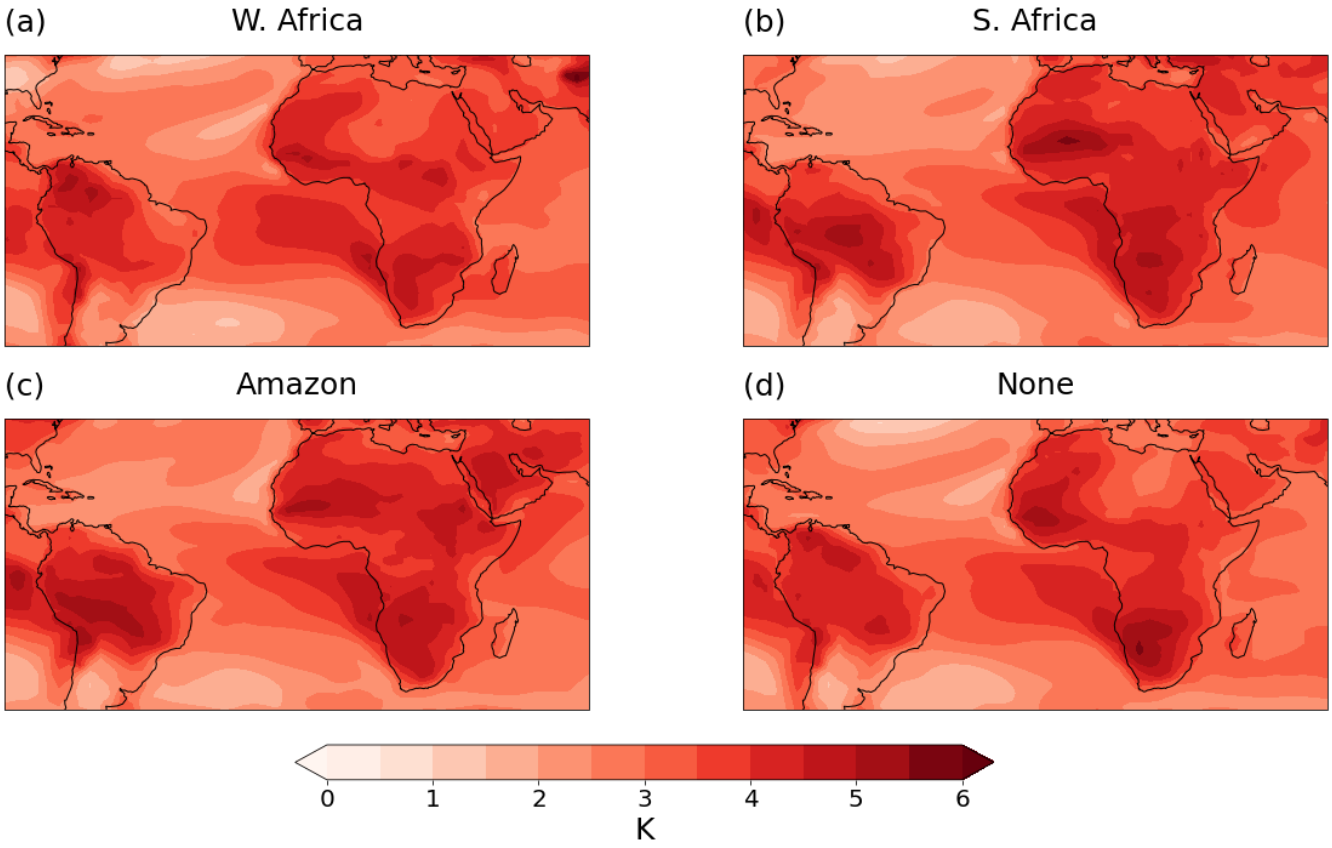


**S3: The multimodel mean change in surface temperature for the period 2090–2100 for (a) the Western African burning season (Dec–Feb), (b) the Southern African burning season (June, July), (c) the Southern Amazon burning season (Aug–Oct), and (d) the remaining months with limited burning (March–May, Nov).**

## S4: The relationship between NOx and ozone production

To evaluate the sensitivity of ozone production rate to changes in NOx concentration and isoprene emission rate due to climate change, we test several ordinary least squares linear regression models (Table S3). We evaluate percentage changes (labelled as VARIABLE (%) in Table S3) and absolute changes. For the absolute changes, the predictor variables are standardised. Finally, we test whether the $r^2$ value increases with different predictor variables. In Table S3, 'Δnox' is the change in NOx concentration, 'Δisop' is the change in isoprene emission rate and 'nox' is the background concentration of NOx. The qq-plots in Fig. S4 show the distribution of the residuals for the model lm(Δprod (%) ~ Δnox (%) + Δisop (%)). Although the residuals are overdispersed, the large sample size allows us to rely on central limit theorem to interpret the significance of results.

Both the change in NOx due to climate change, and the background concentration of NOx are important for predicting the change in ozone production rate, especially in UKESM1 as the $r^2$ value increases from 0.211 to 0.458 with the addition of NOx

as a predictor variable. This relationship is shown for UKESM1 in Fig. S2a; ozone production increases with NOx concentration change at very low NOx, but when background NOx is high, ozone production increases with background NOx even when the change in NOx concentration is negative. The change in ozone production in GISS and MRI are more strongly correlated with the change in NOx concentration (Fig. S2a, S2b), although including background NOx as a predictor variable improved the $r^2$ values (0.345 to 0.618 for MRI and 0.683 to 0.78- for GISS, Table S3). This difference between UKESM1 and the other two models may be because UKESM1 has much higher NOx concentrations than GISS and MRI. Doherty et al. (2013) has previously found that ozone production rate in UM-CAM was strongly related to background NOx concentration whereas GISS-PUCCINI, which had lower NOx concentrations, was less strongly related.

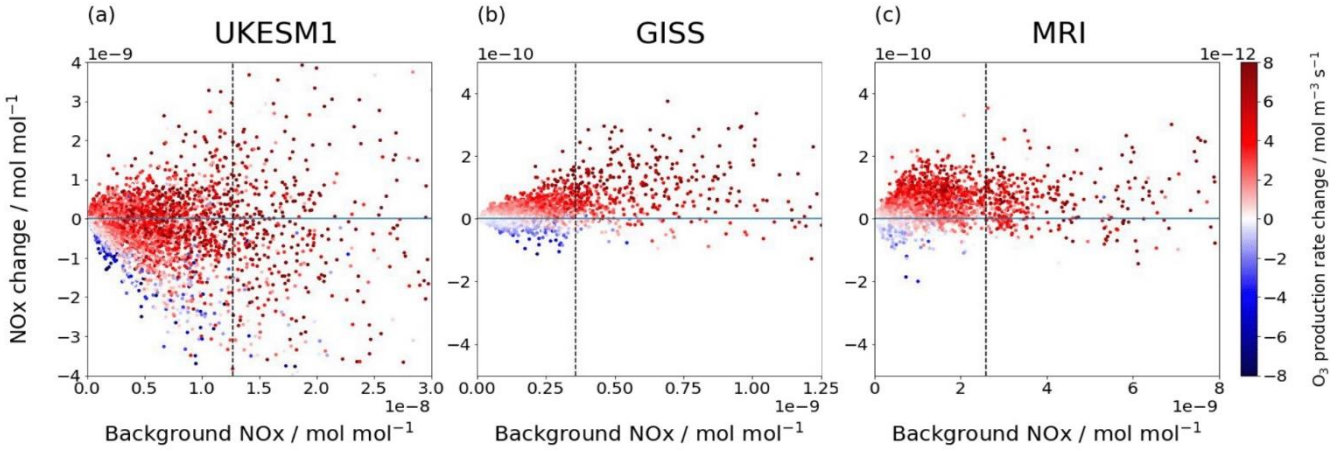


**Figure S4: Scatter plots of the monthly mean background surface NOx concentration, change in NOx concentration due to climate change and change in ozone production rate due to climate for each grid cell and each month for (a) UKESM1, (b) GISS and (c) MRI. The 95th percentile for background NOx concentration is marked with a dashed black line in each case.**

| | Model | $r^2$ | AIC |
|---|---|---|---|
| UKESM1 | lm(Δprod (%) ~ Δnox (%)) | 0.384 | -2.403e+04 |
| GISS | lm(Δprod (%) ~ Δnox (%)) | 0.696 | 4.610e+04 |
| MRI | lm(Δprod (%) ~ Δnox (%)) | 0.590 | -1.937e+04 |
| UKESM1 | lm(Δprod (%) ~ Δnox (%) + Δisop (%)) | 0.384 | - 2.393e+04 |
| GISS | lm(Δprod (%) ~ Δnox (%) + Δisop (%)) | 0.732 | 4.527e+04 |
| MRI | lm(Δprod ~ Δnox) | 0.345 | 1.292e+04 |
| UKESM1 | lm(Δprod ~ Δnox + Δisop) | 0.211 | 3.813e+04 |

| | | | |
|---|---|---|---|
| GISS | lm(Δprod ~ Δnox + Δisop) | 0.685 | 1.101e+04 |
| MRI | lm(Δprod ~ Δnox + nox) | 0.618 | 1.005e+04 |
| UKESM1 | lm(Δprod ~ Δnox + Δisop + nox) | 0.458 | 3.261e+04 |
| GISS | lm(Δprod ~ Δnox + Δisop + nox) | 0.780 | 8667 |

**Table S4: $r^2$ and AIC values for linear regression models using different predictor variables to test correlation with the change in ozone production due to climate change. The '%' in column 2 indicates that the variables have been converted to a percentage change.**

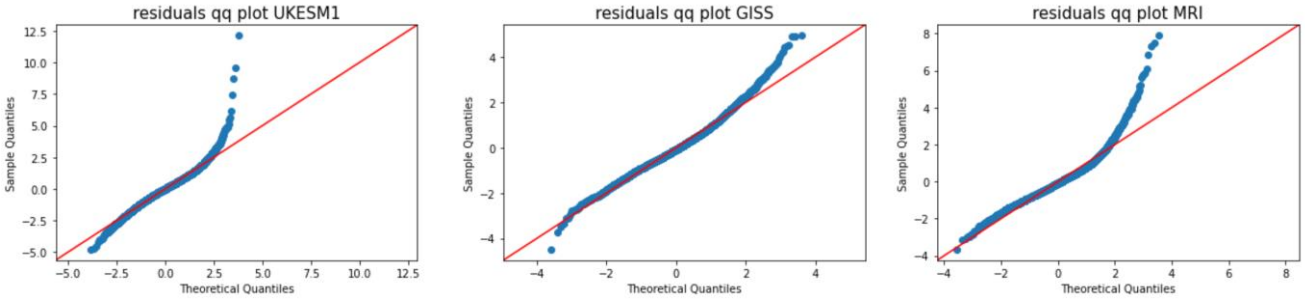


**Figure S5: QQ plots of the standardised residuals for (a) UKESM1, (b) GISS and (c) MRI for the linear model lm(Δprod (%) ~ Δnox (%) + Δisop (%)). For MRI Δisop (%) = 0 so the model lm(Δprod (%) ~ Δnox (%) ) is used.**

## S5: Chemical loss rates

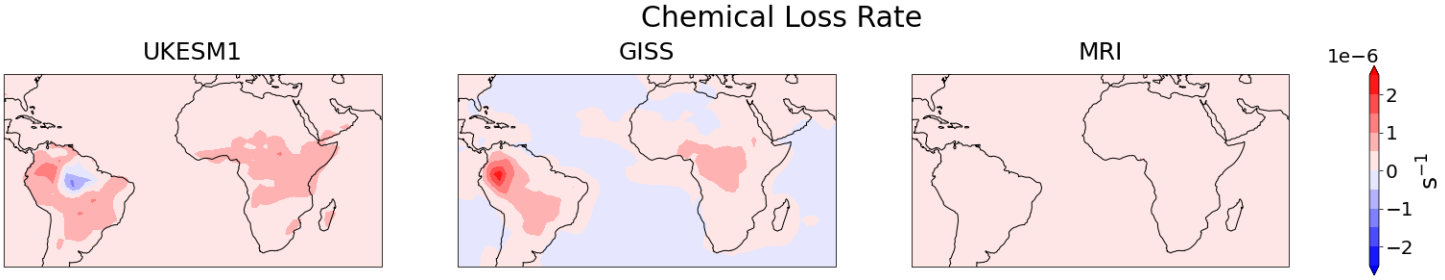


**Figure S6: The average change due to climate change in ozone chemical loss rate for the period 2090 - 2100 for (a) UKESM1, (b) GISS and (c) MRI.**

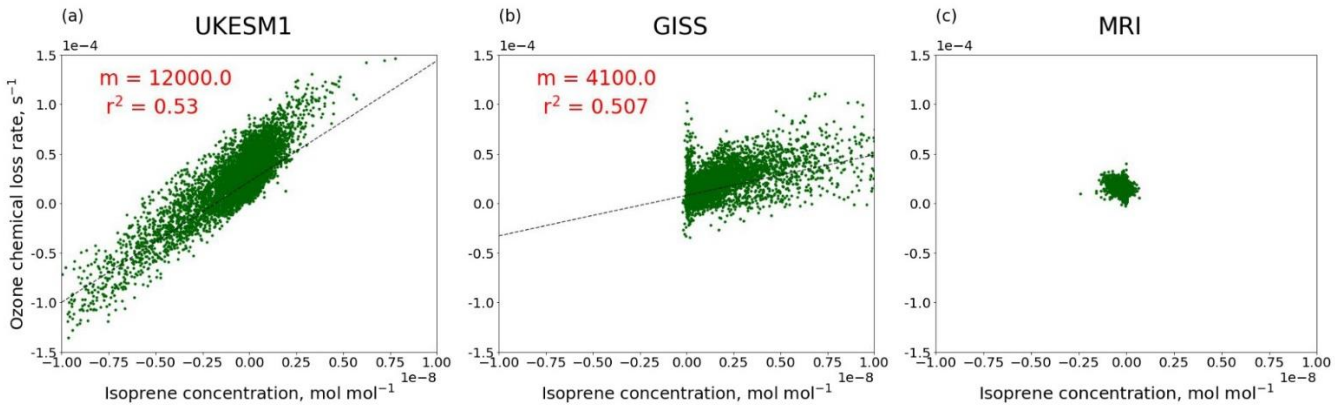


**Figure S7: The relationship between the change in isoprene concentration and the rate of ozone chemical loss over the land surface for (a) UKESM, (b) GISS and (c) MRI. A line of best fit is included for (a) and (b) with gradient *m* and an $r^2$ value.**